Microenvironment and Immunology

Cancer Research

Tuning Sensitivity of CAR to EGFR Density Limits Recognition of Normal Tissue While Maintaining Potent Antitumor Activity

Hillary G. Caruso[1,2], Lenka V. Hurton[1,2], Amer Najjar[1], David Rushworth[1,2], Sonny Ang[1], Simon Olivares[1], Tiejuan Mi[1], Kirsten Switzer[1], Harjeet Singh[1], Helen Huls[1], Dean A. Lee[1,2], Amy B. Heimberger[3], Richard E. Champlin[4], and Laurence J.N. Cooper[1,2]

Abstract

Many tumors overexpress tumor-associated antigens relative to normal tissue, such as EGFR. This limits targeting by human T cells modified to express chimeric antigen receptors (CAR) due to potential for deleterious recognition of normal cells. We sought to generate CAR$^+$ T cells capable of distinguishing malignant from normal cells based on the disparate density of EGFR expression by generating two CARs from monoclonal antibodies that differ in affinity. T cells with low-affinity nimotuzumab-CAR selectively targeted cells overexpressing EGFR, but exhibited diminished effector function as the density of EGFR decreased. In contrast, the activation of T cells bearing high-affinity cetuximab-CAR was not affected by the density of EGFR. In summary, we describe the generation of CARs able to tune T-cell activity to the level of EGFR expression in which a CAR with reduced affinity enabled T cells to distinguish malignant from nonmalignant cells. *Cancer Res; 75(17); 3505–18. ©2015 AACR.*

Introduction

T cells genetically modified to express a chimeric antigen receptor (CAR) to redirect specificity for desired tumor-associated antigen (TAA) can be infused into patients as immunotherapy. Because many TAAs overexpressed on tumors also have low density expression on normal tissue, use of CAR-modified T cells to specifically target such antigens has been limited by the potential for on-target, normal tissue toxicity. Indeed, prolonged B-cell aplasia in patients with B-lineage leukemias and lymphomas after infusion of CD19-specifc CAR$^+$ T cells highlights inability to distinguish between CD19 on malignant and normal B cells (1–3).

Glioblastoma (GBM) is the most common and aggressive malignancy of the brain and central nervous system with a median survival of approximately 1 year from diagnosis (4, 5). EGFR is aberrantly overexpressed in more than 60% of adult GBM and contributes to tumor progression by promoting cell division, invasion, angiogenesis, and inhibiting apoptosis (6). Clinical efforts to target EGFR on GBM with tyrosine kinase inhibitors (TKI) and monoclonal antibodies (mAb) have had limited success, apparently due to signaling through compensatory pathways and poor blood–brain barrier penetration (7, 8). Furthermore, targeting EGFR via TKIs or mAb can cause toxicity, primarily observed in skin, gastrointestinal system, and kidney, due to distribution of EGFR on these normal tissues (9, 10).

EGFR is overexpressed on GBM relative to normal cells, which raises the possibility that CAR$^+$ T cells may be generated to distinguish malignant from normal cells based on EGFR density. This is based upon published observations that T-cell activation initiated through the endogenous αβ T-cell receptors (TCR) can be triggered by binding of a few high-affinity TCRs or greater numbers of low-affinity TCRs (11, 12). We hypothesized that the affinity of a single-chain variable fragment (scFv), which imparts CAR specificity, may impact the effector response to the density of EGFR, such that T cells would be activated when docked with overexpressed EGFR on tumor cells and not with low, basal EGFR expression on normal cells.

To accomplish this, we derived two CAR species from cetuximab and nimotuzumab, which bind to highly overlapping epitopes on EGFR, yet exhibit different affinities (13). Nimotuzumab has a 10-fold lower K_d than cetuximab resulting from a 59-fold reduced on-rate of binding, which imparts a requirement for (at least) bivalent binding to EGFR and restricts the binding to cells expressing high-density EGFR (13–15). Therefore, we generated two second generation EGFR-specific CARs, which derive their specificity from the scFv regions of nimotuzumab-CAR or cetuximab-CAR, and are activated by chimeric CD28 and CD3-ζ cytosolic domains. We observed that T cells could be fully activated by both nimotuzumab-CAR and cetuximab-CAR when EGFR was expressed at high density on glioma cells. However, at reduced levels of EGFR expression, the lower affinity

[1]Division of Pediatrics, The University of Texas MD Anderson Cancer Center, Houston, Texas. [2]The University of Texas Graduate School of Biomedical Sciences at Houston, Houston, Texas. [3]Department of Neurosurgery, The University of Texas MD Anderson Cancer Center, Houston, Texas. [4]Department of Stem Cell Transplantation and Cellular Therapy, The University of Texas MD Anderson Cancer Center, Houston, Texas.

Note: Supplementary data for this article are available at Cancer Research Online (http://cancerres.aacrjournals.org/).

Corresponding Author: Laurence J.N. Cooper, The University of Texas MD Anderson Cancer Center, 7455 Fannin Street, Unit 907, Houston, TX 77054. Phone: 713-301-5041; Fax: 713-792-9832; E-mail: ljncooper@mdanderson.org; ljncooper@ziopharm.com

doi: 10.1158/0008-5472.CAN-15-0139

nimotuzumab-CAR$^+$ T cells exhibited reduced T-cell activation while cetuximab-CAR$^+$ T cells maintained efficient activation independent of EGFR density. In summary, we describe a strategy to engineer T cells to distinguish tumor from normal cells based on tuning the functional affinity of CAR to selectively target cells overexpressing EGFR.

Materials and Methods

DNA plasmids

The derivation of cetuximab-CAR and nimotuzumab-CAR is described in Supplementary Materials and Methods. Cetuximab-CAR and nimotuzumab-CAR were cloned as *Sleeping Beauty* (SB) transposons under control of hEF1-α promoter, as previously described (16). Codon-optimized truncated human EGFR (amino acids 1-668, NP_005219.2; GeneArt) was cloned under expression of hEF1-α promoter followed by F2A cleavable peptide and neomycin phosphotransferase. CAR-L was derived from hybridoma clone 2D3 (17).

Cell lines

Cell lines obtained from ATCC include EL4 (2009), NALM-6 (2011), U87 (2012), T98G (2012), LN18 (2012), and A431 (2012). K562 clone 9 were generated by stable expression of 41BB-L, CD86, CD64, and tCD19 (18) and were a kind gift from Dr. Carl June (University of Pennsylvania, Philadelphia, PA), obtained in 2007. U87-172b cells, designated U87^{high} in this study, overexpressing wild-type EGFR were a kind gift from Dr. Oliver Bolger (The University of Texas MD Anderson Cancer Center, Houston, TX) and obtained in 2012. Human renal cortical epithelial (HRCE) cells were obtained from Lonza in 2012. Details of propagation and genetic modification are described in Supplementary Materials and Methods. All cell line identities were validated by STR DNA fingerprinting in 2012, at the time of the study, using the AmpF_STR Identifier kit according to manufacturer's instructions (Applied Biosystems, cat. #4322288). The STR profiles were compared to known ATCC fingerprints (ATCC.org), and to the Cell Line Integrated Molecular Authentication database (CLIMA) version 0.1.200808 (19). The STR profiles matched known DNA fingerprints.

T-cell modification and culture

Peripheral blood mononuclear cells (PBMC) from healthy donors were purchased from Gulf Coast Regional Blood Bank and isolated by Ficoll-Paque (GE Healthcare) and cryopreserved. T cells were cultured in RPMI1640 (HyClone) supplemented with 10% FBS (HyClone) and 2 mmol/L Glutamax (Gibco). Electrotransfer of SB plasmids coding for CAR is detailed in Supplementary Materials and Methods and as previously described (16).

Surface immunostaining and flow cytometry

Data were collected on FACS Calibur (BD Biosciences) using CellQuest software (version 3.3, BD Biosciences) and analyzed using FlowJo software (version x.0.6, TreeStar). Up to 10^6 cells were stained with mAbs (Supplementary Table S1) in FACS buffer (PBS, 2% FBS, 0.5% sodium azide) for 30 minutes in the dark at 4°C. Quantitative flow cytometry was performed using Quantum Simply Cellular polystyrene beads, according to manufacturer's instructions (cat. #814; Bangs Laboratories) using mAb specific for EGFR (cat. #555997; BD Biosciences). A standard curve relating mean fluorescence intensity to EGFR molecules/cell was made using QuickCal Data Analysis Program (version 2.3, Bangs Laboratories). EGFR molecules/cell was calculated by subtracting MFI of isotype antibody from MFI of EGFR and extrapolating from standard curve.

Intracellular cytokine production

T cells were cocultured with target cells at a ratio of 1:1 for 4 to 6 hours in the presence of GolgiStop diluted 1:4,000 (cat. #554724, BD Biosciences). T cells treated with Leukocyte Activation Cocktail (cat. #550583, BD Biosciences) diluted 1:1,000 served as positive control. An EGFR-specific mAb (clone LA1, Millipore) was used to block binding of CAR$^+$ T cells with EGFR on target cells at a concentration of 5 μg/mL. Following incubation, surface staining and intracellular cytokine staining were performed using Cytofix/Cytoperm Fixation and Permeabilization Kit (cat. #554714, BD Biosciences) according to manufacturer's instructions.

Phospho-flow cytometry

T cells were cocultured with target cells at a ratio of 1:1 for 45 minutes, then lysed and fixed using PhosFlow Lyse/Fix buffer (cat. #558049, BD Biosciences), detailed in Supplementary Materials and Methods, and analyzed via flow cytometry.

Measurement of downregulation of CAR expression

T cells and targets were mixed at a 1:1 ratio in a 12-well plate and CAR surface expression was measured by flow cytometry at each time point. T cells plated without targets served as negative controls. Percent downregulation of CAR was calculated as: (stimulated CAR expression)/(unstimulated CAR expression) × 100.

Chromium release assay

Specific cytotoxicity was assessed via standard 4-hour chromium release assay, as previously described (16).

Evaluation of T-cell efficacy in intracranial glioma xenograft

Animal experiments were carried out under regulation from the Institutional Animal Care and Use Committee at The University of Texas MD Anderson Cancer Center (ACUF 11-11-13131). Female NOD.Cg-Prkdc^{scid}IL2Rγ^{tm1Wjl}/Sz (NSG, Jackson Laboratory) mice aged 6 to 8 weeks were anesthetized by intraperitoneal injection of 100 mg/kg ketamine and 5 mg/kg xylazine. Implantation of guide screw is detailed in Supplementary Materials and Methods. Two weeks following guide screw implantation, 250,000 U87-ffLuc-mKate or U87^{med}-ffLuc-mKate cells were implanted through guide screw in 5 μL PBS. Burden of intracranial glioma was serially imaged using Xenogen IVIS Spectrum (Caliper Life Sciences) 10 minutes after subcutaneous injection of 215 μg D-luciferin potassium salt (cat. #122796, Caliper Life Sciences). Tumor flux (photons/s/cm^2/steradian) was measured using Living Image software (version 2.50, Caliper Life Sciences) in a delineated region encompassing entire cranial region. Mice were stratified into three groups to evenly distribute tumor burden based on bioluminescent imaging (BLI) measurements 4 days after tumor injection and treated with 4×10^6 T cells administered once a week for three weeks through the guide screw in 5 μL of PBS. Mice were sacrificed when they displayed progressive weight loss (>25% loss), rapid weight loss (>10% loss within 48 hours), hind limb paralysis, or any two of the following clinical symptoms of illness: ataxia, hunched posture, irregular respiration rate, ulceration of exposed tumor, or palpable tumor diameter exceeding 1.5 cm.

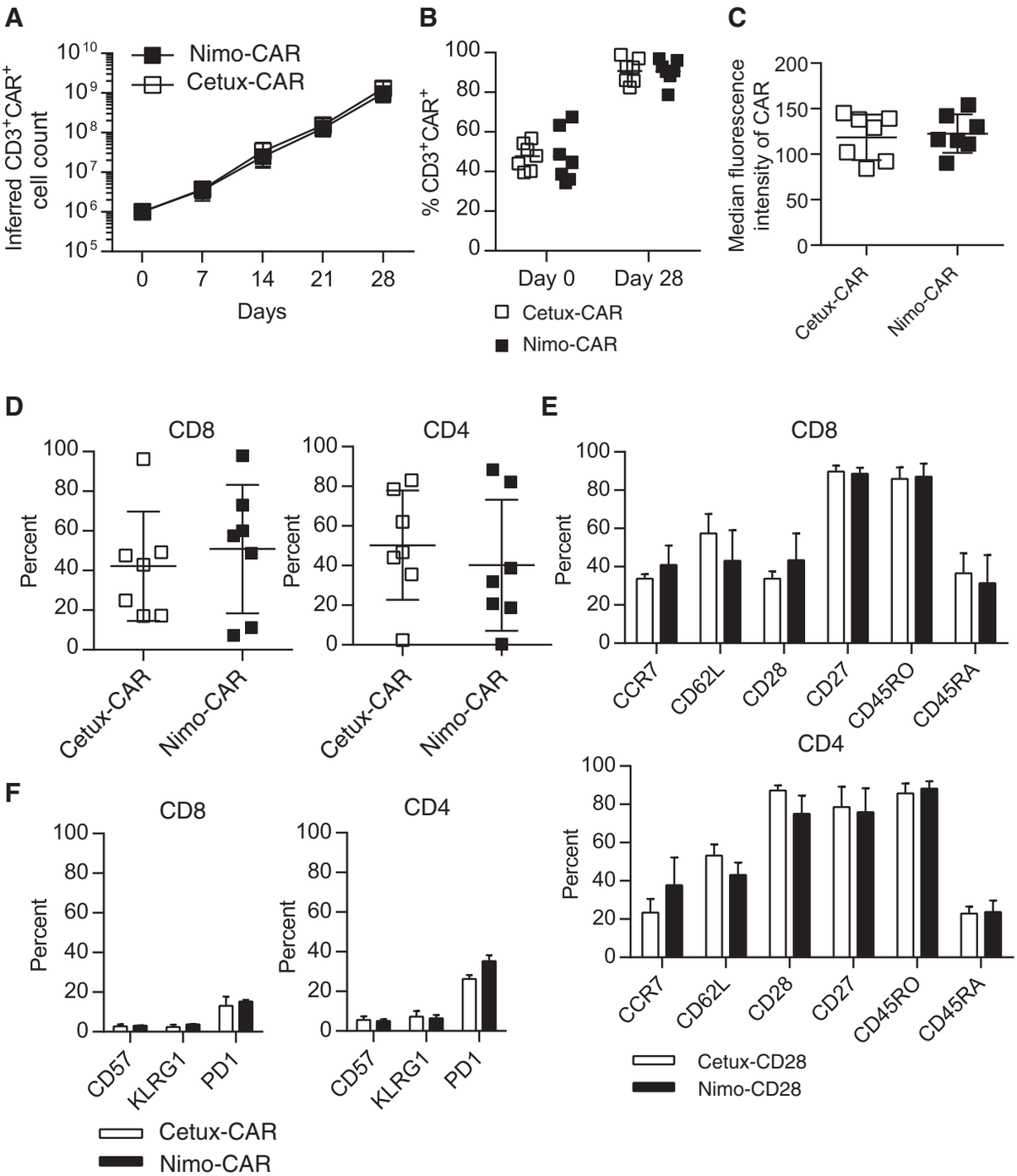

Figure 1.
Cetuximab-CAR$^+$ (Cetux-CAR$^+$) and nimotuzumab-CAR$^+$ (Nimo-CAR$^+$) T cells are phenotypically similar. A, numeric expansion of cetuximab-CAR$^+$ and nimotuzumab-CAR$^+$ T cells was determined by calculating fold expansion of CD3$^+$CAR$^+$ T cells, determined by flow cytometry, during each stimulation cycle. Data, mean ± SD, $n = 5$. Statistical analysis by a two-tailed Student t test. B, expression of CAR in CD3$^+$ T cells was determined 24 hours after electroporation of CAR and after 28 days of expansion by flow cytometry for the IgG portion of CAR. Data, mean, $n = 7$. Statistical analysis performed by a two-tailed Student t test. C, median fluorescence intensity (MFI) of CAR expression was determined by flow cytometry for the IgG portion of CAR after 28 days of expansion. Data, mean ± SD, $n = 7$. Statistical analysis performed by a two-tailed Student t test. D, proportion of CD4 and CD8 T cells in total T-cell population after 28 days of expansion measured by flow cytometry on gated CD3$^+$CAR$^+$ cells. Data, mean ± SD, $n = 7$. Statistical analysis performed by a two-tailed Student t test. E and F, expression of T-cell memory and differentiation markers after 28 days of T-cell expansion measured by flow cytometry in gated CD4$^+$ and CD8$^+$ T-cell populations. Data, mean ± SD, $n = 4$. Statistical analysis performed by two-way ANOVA with the Sidak post-test correction.

Statistical analyses

Statistical analyses were performed in GraphPad Prism, version 6.03. Statistical analyses of *in vitro* assays were undertaken by two-way ANOVA with donor-matching and Sidak or Tukey post-test for multiple comparisons or two-tailed Student *t* test, as indicated in Figure legends. Correlation of T-cell effector functions with EGFR density was performed by one-way ANOVA with post-test for linear trend. Analyses of *in vivo* BLI of tumor were performed using two-way ANOVA with repeated measures and Sidak post-test for multiple comparisons. Survival of mice was performed by the log-rank (Mantel–Cox) test. Significance of findings defined as follows: ns = not significant; $P > 0.05$; *, $P < 0.05$; **, $P < 0.01$; ***, $P < 0.001$; ****, $P < 0.0001$.

Results

Cetuximab-CAR$^+$ and nimotuzumab-CAR$^+$ T cells are phenotypically similar

Cetuximab-CAR and nimotuzumab-CAR were generated in SB vectors (Supplementary Fig. S1A), expressed in T cells via electroporation, and propagated by weekly stimulations with EGFR$^+$ activating and propagating cells (AaPC; Supplementary Fig. S1B). Cetuximab- and nimotuzumab-CAR$^+$ T cells expanded approximately 1,000-fold over 28 days (Fig. 1A). There was no difference in the kinetics or number of resultant T cells ($P = 0.92$), and similar CAR expression (cetuximab-CAR = 91% ± 6%, nimotuzumab-CAR = 91% ± 6%; mean ± SD, $n = 7$; Fig. 1B). The density of CAR expression, represented by median fluorescence intensity, was statistically similar on cetuximab-CAR$^+$ and nimotuzumab-CAR$^+$ T-cell populations [cetuximab-CAR = 119 ± 25 arbitrary units (A.U.), nimotuzumab-CAR = 113 ± 21 A.U.; mean ± SD, $n = 7$, $P = 0.74$; Fig. 1C)]. While individual donors yielded variable proportions of CD4$^+$ and CD8$^+$ T cells (Supplementary Table S2), there was no statistical difference in the CD4/CD8 ratio between cetuximab-CAR$^+$ and nimotuzumab-CAR$^+$ T cells ($P = 0.44$; Fig. 1D). Expression of cell-surface markers associated with T-cell differentiation (CD45RO, CD45RA, CD28, CD27, CCR7, CD62L, CD57, KLRG1, and PD-1) were not significantly different ($P > 0.05$; Fig. 1E and F).

To verify cetuximab-CAR and nimotuzumab-CAR were functional in response to EGFR stimulation, we measured production of the inflammatory cytokine IFNγ in response to A431, an epidermoid carcinoma cell line expressing approximately 1×10^6 molecules of EGFR/cell (20). Both cetuximab-CAR$^+$ and nimotuzumab-CAR$^+$ T cells produced IFNγ in response to A431 and production was titrated in response to an EGFR-blocking antibody (clone LA1, Millipore) with an overlapping epitope (Fig. 2B and C). Reduction in IFNγ production by nimotuzumab-CAR$^+$ T cells was observed at lower concentrations of antibody than cetuximab-CAR$^+$ T cells, supporting that differences in scFv

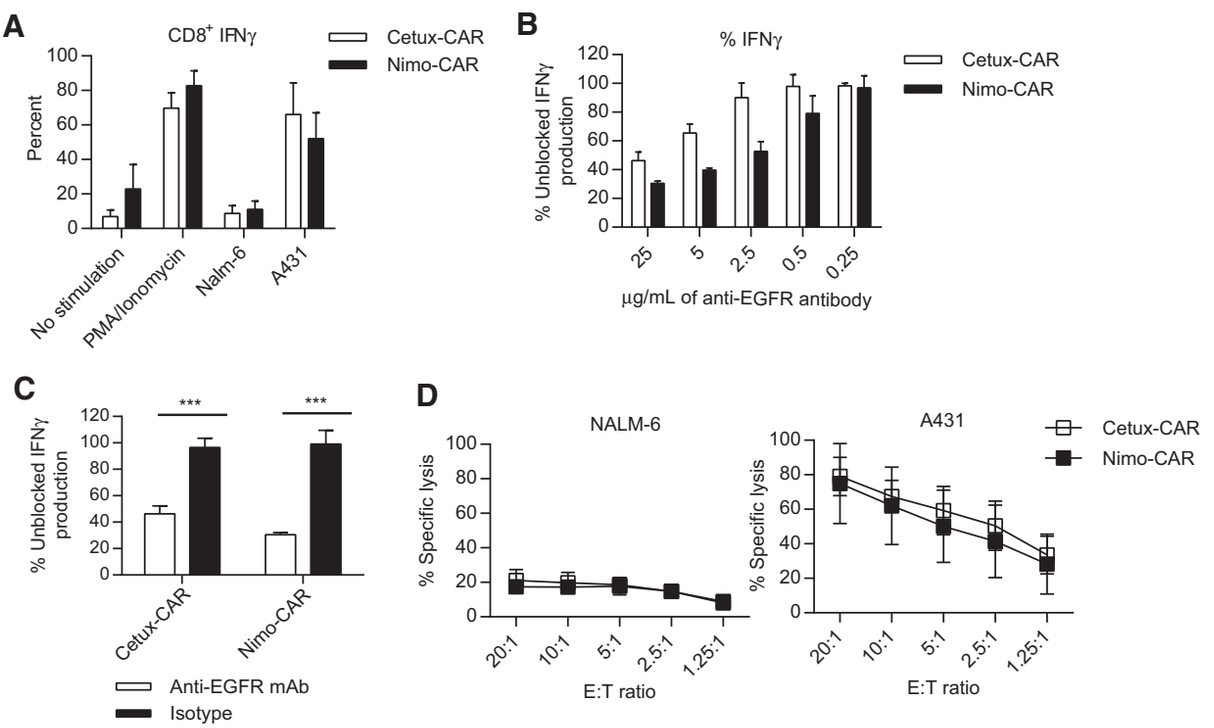

Figure 2.
Cetuximab-CAR$^+$ (Cetux-CAR$^+$) and nimotuzumab (Nimo-CAR$^+$) T cells are activated in response to EGFR. A, production of IFNγ by CD8$^+$CAR$^+$ T cells in response to coculture with A431 and NALM-6 cell lines measured by intracellular flow cytometry gated on CD8$^+$ cells. Data, mean ± SD, $n = 4$; ***, $P < 0.001$, two-way ANOVA (Sidak post-test). B, production of IFNγ in response to EGFR$^+$ A431 in the presence of titrating concentrations of EGFR-blocking mAb (clone LA1, Millipore). CAR$^+$ T cells were cocultured with A431 with EGFR-specific mAb and IFNγ production was measured by intracellular flow cytometry. Percent of production was calculated as mean fluorescence intensity of IFNγ in gated CD8$^+$ T cells relative to unblocked CD8$^+$ T-cell production. Data, mean ± SD, $n = 3$. C, production of IFNγ as measured by intracellular flow cytometry in response to EGFR$^+$ A431 in the presence 25 μg/mL of EGFR-blocking mAb (clone LA1, Millipore). Percent of production was calculated as mean fluorescence intensity of IFNγ in gated CD8$^+$ T cells relative to unblocked CD8$^+$ T-cell production. Data, mean ± SD, $n = 3$; ***, $P < 0.001$, two-way ANOVA (Sidak post-test). D, specific lysis of A431 and NALM-6 by CAR$^+$ T cells measured by standard 4-hour chromium release assay. Data, mean ± SD, $n = 4$.

binding affinity are preserved in CAR structure. Cetuximab-CAR$^+$ and nimotuzumab-CAR$^+$ T cells both lysed A431 cells, however, neither population significantly lysed EGFR^{neg} NALM-6 cells (Fig. 2D). Cetuximab-CAR$^+$ and nimotuzumab-CAR$^+$ T cells are phenotypically similar, including percentage and density of CAR expression, and are activated upon encounter with EGFR.

Nimotuzumab-CAR$^+$ T cells have impaired response to low-density EGFR

We next determined whether affinity of scFv within the CARs could affect effector functions of genetically modified T cells as a function of density of EGFR expression. The activation of cetuximab-CAR$^+$ and nimotuzumab-CAR$^+$ T cells in response to EL4 cell line genetically modified to express tEGFR (Supplementary Fig. S1C) at a low density, similar to normal human fibroblasts (Fig. 3A; ref. 21), was compared with T-cell activation by EL4 cells capable of cross-linking CARs independently of scFv through expression of CAR-L, an activating scFv of mAb specific for the IgG4-derived domain of CAR (17). A similar proportion of cetuximab-CAR$^+$ and nimotuzumab-CAR$^+$ T cells produced IFNγ in response to CAR-L$^+$ EL4, ($P > 0.05$; Fig. 3B). While cetuximab-CAR$^+$ T cells increased IFNγ production in response to tEGFR$^+$ EL4 relative to tCD19$^+$ EL4

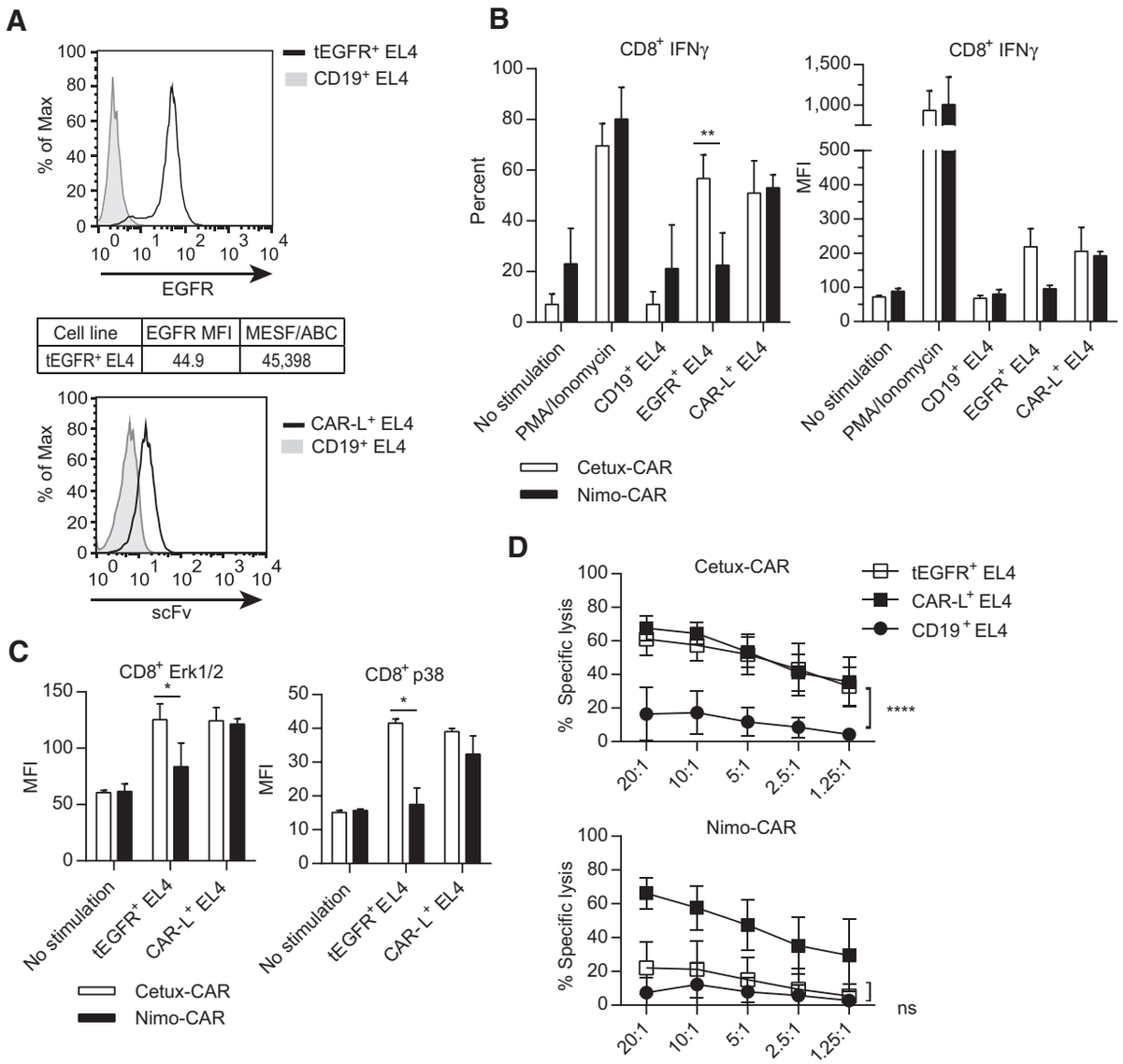

Figure 3.
Nimotuzumab-CAR$^+$ (Nimo-CAR$^+$) T cells have impaired response to low density of EGFR. A, representative histograms of expression of enforced tEGFR and CAR-L on EL4 cells relative to EL4 cells negative for EGFR and CAR-L. Density of EGFR expression was determined by quantitative flow cytometry. B, production of IFNγ by gated CD8$^+$ CAR$^+$ T cells after coculture with CD19$^+$, tEGFR$^+$, or CAR-L$^+$ EL4 cells measured by intracellular staining and flow cytometry. Data, mean percent ± SD, $n = 4$ and mean fluorescence intensity (MFI) ± SD, $n = 2$; **, $P < 0.01$, two-way ANOVA (Sidak post-test). C, phosphorylation of p38 and Erk1/2 by phosflow cytometry in gated CD8$^+$ CAR$^+$ T cells 30 minutes after coculture with CD19$^+$, tEGFR$^+$, or CAR-L$^+$ EL4 cells. Data, mean ± SD, $n = 2$; *, $P < 0.05$, two-way ANOVA (Sidak post-test). D, specific lysis of CD19$^+$, tEGFR$^+$, and CAR-L$^+$ EL4 cells measured by standard 4-hour chromium release assay. Data, mean ± SD, $n = 4$; ****, $P < 0.0001$, two-way ANOVA (Tukey post-test).

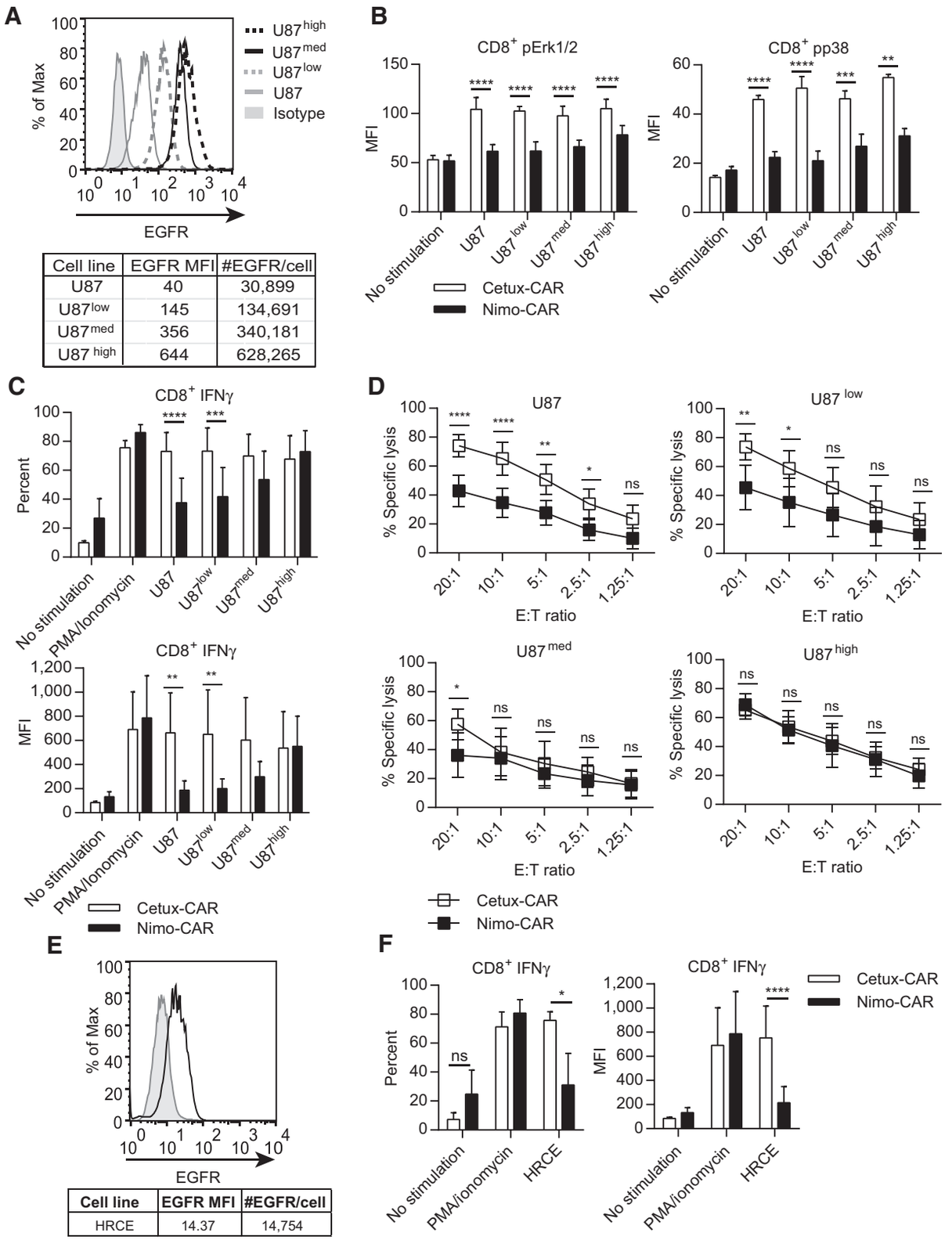

Cell line	EGFR MFI	#EGFR/cell
U87	40	30,899
U87low	145	134,691
U87med	356	340,181
U87 high	644	628,265

Cell line	EGFR MFI	#EGFR/cell
HRCE	14.37	14,754

Figure 4.

Nimotuzumab-CAR$^+$ (Nimo-CAR$^+$) T-cell activation is positively correlated with EGFR density. A, representative histogram of EGFR expression on series of four U87-derived tumor cell lines (U87, U87^{low}, U87^{med}, and U87^{high}) measured and quantified by flow cytometry. Data are representative from triplicates. B, phosphorylation of Erk1/2 and p38 in gated CD8$^+$ T cells after 45 minutes of coculture with U87 cell lines by phosflow cytometry. (*Continued on the following page.*)

(%IFNγ, $P < 0.0001$; MFI IFNγ, $P < 0.01$), nimotuzumab-CAR$^+$ T cells did not (%IFNγ, $P > 0.05$, MFI IFNγ, $P > 0.05$). There was no statistical difference in activation as assessed by phosphorylation of Erk1/2 ($P > 0.05$) or p38 ($P > 0.05$) between cetuximab-CAR$^+$ and nimotuzumab-CAR$^+$ T cells in response to CAR-L$^+$ EL4 (Fig. 3C). In contrast, cetuximab-CAR$^+$ T cells exhibited phosphorylation of Erk1/2 and p38 in response to tEGFR$^+$ EL4, while nimotuzumab-CAR$^+$ T cells did not. Cetuximab-CAR$^+$ and nimotuzumab-CAR$^+$ T cells demonstrated equivalent specific lysis against CAR-L$^+$ EL4 [10:1 effector-to-target (E:T) ratio, cetuximab-CAR = 65% ± 7%, nimotuzumab-CAR = 58% ± 13%, mean ± SD, $n = 4$, $P > 0.05$; Fig. 3D]. However, differences were observed in capacity to lyse tEGFR$^+$ EL4, where cetuximab-CAR$^+$ T cells demonstrated significant lysis of tEGFR$^+$ EL4 compared with irrelevant antigen (tEGFR$^+$EL4 = 58% ± 9%, tCD19$^+$EL4 = 17% ± 13%, mean ± SD, $n = 4$; $P < 0.0001$) and nimotuzumab-CAR$^+$ T cells did not (tEGFR$^+$EL4 = 21% ± 17%, CD19$^+$EL4 = 12% ± 13%, mean ± SD, $n = 4$, $P > 0.05$). These data demonstrate that both CARs are capable of activating T cells when triggered outside of scFv, yet differ in ability to activate T cells to low density EGFR.

Nimotuzumab-CAR$^+$ T-cell activation is positively correlated with EGFR density

We sought to further evaluate the impact of TAA density on activation of CAR T cells in a single cellular background by modifying U87 cells to express varied levels of EGFR, reflective of densities found in GBM cell lines (Fig. 4A; ref. 22): unmodified parental U87, U87^{low}, U87^{med}, and U87^{high}. Phosphorylation Erk1/2 and p38 in cetuximab-CAR$^+$ T cells exhibited no correlation with density of EGFR expression (one-way ANOVA with post-test for linear trend; Erk1/2, $P = 0.88$; p38, $P = 0.09$; Fig. 4B). In contrast, phosphorylation of Erk1/2 and p38 by nimotuzumab-CAR$^+$ T cells positively correlated with EGFR expression (one-way ANOVA with post-test for linear trend; Erk1/2, $P = 0.003$ and p38, $P = 0.004$). We also noted that nimotuzumab-CAR$^+$ T cells demonstrated significantly less phosphorylation of Erk1/2 and p38 compared with cetuximab-CAR$^+$ T cells, even in response to high EGFR density on U87^{high} (Erk1/2, $P < 0.0001$; p38, $P < 0.01$). Percentage and magnitude IFNγ production by cetuximab-CAR$^+$ T cells did not correlate with EGFR density on target cells (one-way ANOVA with post-test for linear trend; %IFNγ, $P = 0.5703$; MFI, $P = 0.9508$) (Fig. 4C). In contrast, both proportion of nimotuzumab-CAR$^+$ T cells producing IFNγ and magnitude of production directly correlated with increasing EGFR density (one-way ANOVA with post-test for linear trend; %IFNγ, $P = 0.0124$; MFI, $P = 0.0175$). Production of TNFα by cetuximab-CAR$^+$ T cells and nimotuzumab-CAR$^+$ T cells showed a similar trend (Supplementary Fig. S2A). Finally, cetuximab-CAR$^+$ T cells demonstrated significantly increased specific lysis of both parental U87 (10:1 E:T ratio, $P < 0.0001$) and U87^{low} (10:1 E:T ratio, $P < 0.05$) targets compared with reduced killing by nimotuzumab-CAR$^+$ T cells. However, there was statistically similar lysis by T cells expressing both CAR designs targeting U87^{med} (10:1 E:T ratio, $P > 0.05$) and U87^{high} (10:1 E:T ratio, $P > 0.05$; Fig. 4D). These data were verified using cell lines with naturally varied EGFR expression (Supplementary Fig. S3). We investigated the ability of CAR T cells to be activated by low density EGFR on normal HRCE, which express approximately 15,000 molecules of EGFR/cell (Fig. 4E). Cetuximab-CAR$^+$ T cells produced IFNγ in response to HRCE (%IFNγ, $P < 0.05$; MFI, $P < 0.01$), whereas nimotuzumab-CAR$^+$ T cells did not (%IFNγ, $P > 0.05$; MFI, $P > 0.05$; Fig. 4F). Similarly, cetuximab-CAR$^+$ T cells, but not nimotuzumab-CAR$^+$ T cells, produced TNFα in response to HRCE (Supplementary Fig. S2B). In summary, cetuximab-CAR$^+$ and nimotuzumab-CAR$^+$ T cells were both activated by target cells expressing high EGFR density, but only nimotuzumab-CAR$^+$ T cells showed diminished activity in response to low EGFR density. These observations support the premise that activation of nimotuzumab-CAR$^+$ T cells, in contrast to cetuximab-CAR$^+$ T cells, is dependent on density of EGFR expression.

Increasing duration of interaction does not restore nimotuzumab-CAR$^+$ T-cell response to low EGFR density

Because low-affinity TCR-mediated responses may be activated by prolonged interaction with antigen in context of MHC (23, 24), we extended the duration of interaction of nimotuzumab-CAR$^+$ T cells with targets to 24 hours, based on demonstrations of saturated maximal killing at this time point in nonradioactive lysis assays (25, 26). Over 24 hours of interaction, nimotuzumab-CAR$^+$ T cells failed to significantly produce IFNγ in response to U87, however, maintained similar IFNγ production to cetuximab-CAR$^+$ T cells in response to U87^{high} (Fig. 5A). Furthermore, cetuximab-CAR$^+$ and nimotuzumab-CAR$^+$ T cells demonstrated a statistically similar ability to control the growth of U87^{high} tumor cells in long-term coculture; however, nimotuzumab-CAR$^+$ T cells were unable to control parental U87 growth (Fig. 5B). While cetuximab-CAR$^+$ T cells demonstrated moderate, similar proliferation in response to U87 and U87^{high}, nimotuzumab-CAR$^+$ T cells demonstrated significantly higher proliferation in response to U87^{high} cells than parental U87 (Fig. 5C). In aggregate, these data show that reduced activation of nimotuzumab-CAR$^+$ T cells to low density EGFR is not restored by increasing duration of interaction.

Cetuximab-CAR exhibits enhanced downregulation upon EGFR docking

The cell surface expression of endogenous TCR and CAR may be decreased following interaction with antigen, and for endogenous TCR, the degree of downregulation is correlated with the strength of TCR binding (27). We investigated whether cetuximab-CAR$^+$ and nimotuzumab-CAR$^+$ T cells have differing propensities for TAA-induced downregulation. When cocultured with parental U87, cetuximab-CAR was reduced from T-cell surface after 12 hours and returned by 48 hours, but expression of nimotuzumab-CAR did not appreciably reduce from the cell surface (Fig. 5D). In response to

(*Continued.*) Data, mean fluorescence intensity (MFI) ± SD, $n = 4$; ****, $P < 0.0001$; ***, $P < 0.001$; **, $P < 0.01$, two-way ANOVA (Sidak post-test). C, production of IFNγ by gated CD8$^+$ CAR$^+$ T cells in response to coculture with U87 cell lines measured by intracellular staining and flow cytometry. Data, mean percent ± SD and mean fluorescence intensity ± SD, $n = 4$; ****, $P < 0.0001$; ***, $P < 0.001$; **, $P < 0.01$, two-way ANOVA (Sidak post-test). D, specific lysis of U87 cell lines by CAR$^+$ T cells measured by standard 4-hour chromium release assay. Data, mean ± SD, $n = 5$; ****, $P < 0.0001$; **, $P < 0.01$; *, $P < 0.05$, two-way ANOVA (Tukey post-test). E, representative histogram of expression of EGFR on HRCE measured by flow cytometry. Number of EGFR molecules per cell determined by quantitative flow cytometry. Data are representative of triplicates. F, production of IFNγ by CD8$^+$ CAR$^+$ T cells after coculture with HRCE measured by intracellular staining and flow cytometry gated on CD8$^+$ cells. Data, mean percentage ± SD and mean fluorescence intensity ± SD, $n = 4$; **, $P < 0.01$; *, $P < 0.05$; ns, nonsignificant, $P > 0.05$, two-way ANOVA (Sidak post-test).

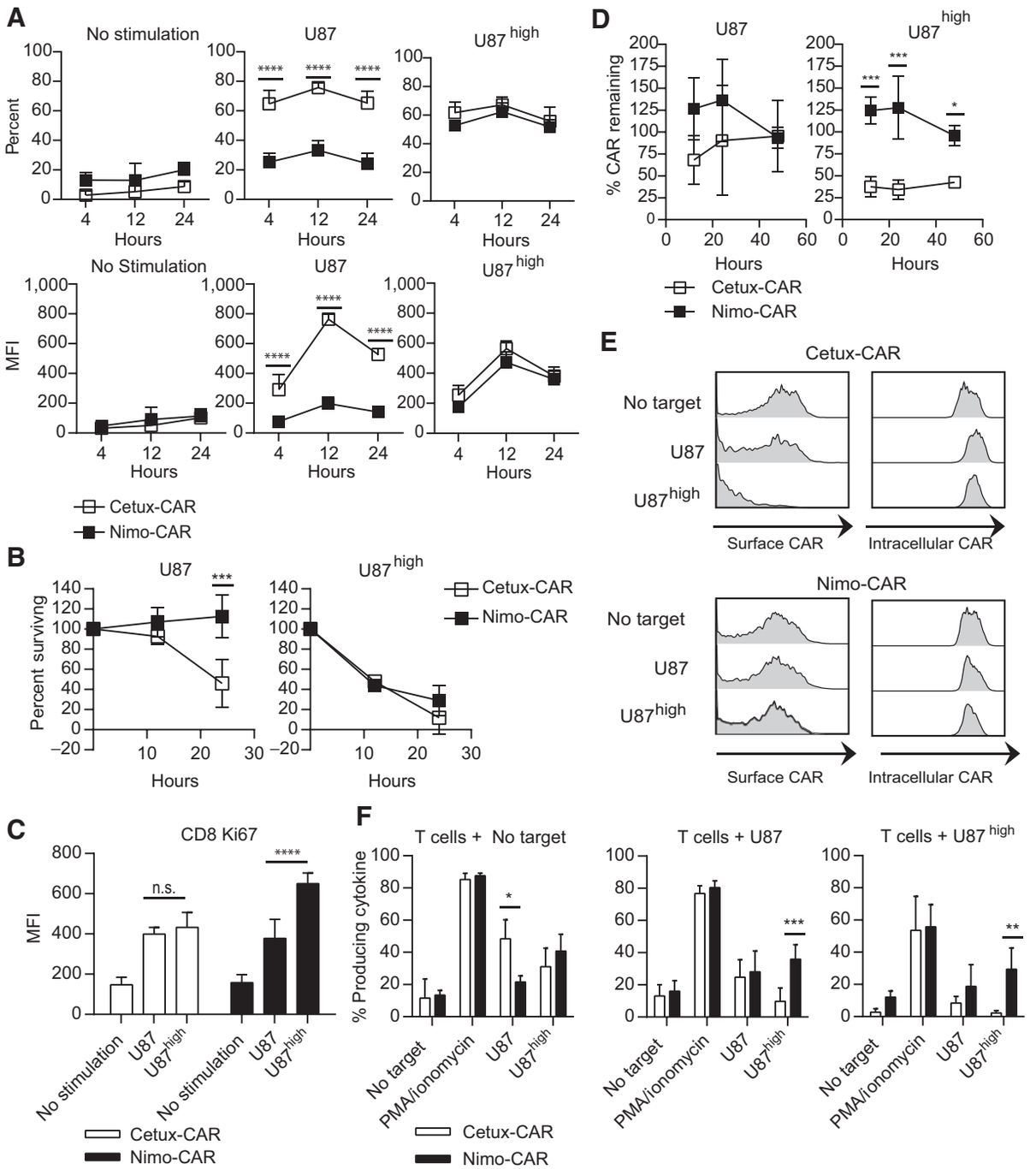

Figure 5.
Increasing duration of interaction does not restore nimotuzumab-CAR$^+$ (Nimo-CAR$^+$) T-cell response to low EGFR density. A, production of IFNγ was measured by intracellular staining and flow cytometry following stimulation with U87 or U87^{high} over time in CD8$^+$ gated cells. Data, mean percent producing ± SD, $n = 4$ and mean fluorescence intensity (MFI) of IFNγ ± SD, $n = 4$; ****, $P < 0.0001$, two-way ANOVA (Sidak post-test). B, fraction of U87 and U87^{high} cells remaining after coculture with cetuximab-CAR$^+$ (Cetux-CAR$^+$) or nimotuzumab-CAR$^+$ (Nimo-CAR$^+$) T cells. U87 cell lines were cocultured with CAR$^+$ T cells at an E:T ratio of 1:5 in triplicate. Percent surviving was calculated as (cell number harvested after coculture)/(cell number without T cells)×100. Data, mean ± SD, $n = 3$; ***, $P < 0.001$, two-way ANOVA (Sidak post-test). C, proliferation of CAR$^+$ T cells measured by intracellular flow cytometry for Ki-67 in CD8$^+$ gated T cells following 36 hours of coculture. Data, mean fluorescence intensity of Ki-67 ± SD, $n = 4$; ***, $P < 0.001$, two-way ANOVA (Tukey post-test). D, surface expression of CAR during coculture (E:T 1:5) with parental U87 or U87^{high} measured by flow cytometry for IgG portion of CAR. Data, mean ± SD, $n = 3$; ***, $P < 0.001$; *, $P < 0.05$, two-way ANOVA (Sidak post-test). E, representative histograms of intracellular and surface expression of CAR determined by flow cytometry after 24 hours of coculture with U87 or U87^{high} in CD8$^+$ gated T cells. Data representative of three independent donors. F, after 24 hours of incubation with U87 or U87^{high}, CAR$^+$ T cells were rechallenged with U87 or U87^{high} and production of IFNγ CAR$^+$ T cells measured by intracellular staining and flow cytometry gated on CD8$^+$ cells. Data, mean ± SD, $n = 3$; ***, $P < 0.001$; **, $P < 0.01$; *, $P < 0.05$, two-way ANOVA (Sidak post-test).

high EGFR density on U87^{high}, cetuximab-CAR was significantly reduced after 12 hours of coculture and remained reduced over 48 hours. Again, nimotuzumab-CAR did not appreciably downregulate (12 hours; cetuximab-CAR = 37% ± 12%, nimotuzumab-CAR = 124% ± 15%, mean ± SD, $n = 3$). Cetuximab-CAR was detectable within T cells when reduced from the T-cell surface, demonstrating that reduced CAR expression was due to internalization of CAR and not outgrowth of genetically unmodified T cells (Fig. 5E). Similarly, when stimulated with tEGFR$^+$ EL4, cetuximab-CAR is reduced from T-cell surface, but nimotuzumab-CAR is not, and both CARs are downregulated to a similar degree when stimulated with CAR-L$^+$ EL4 (Supplementary Fig. S4). To determine whether downregulation of CAR impacts subsequent activation to antigen, we rechallenged CAR$^+$ T cells after initial encounter with EGFR. While cetuximab-CAR$^+$ T cells had reduced production of IFNγ, nimotuzumab-CAR$^+$ T cells retained IFNγ production in response to rechallenge with the glioma cells expressing low and high levels of EGFR (Fig. 5F). Thus, downregulation of CAR is a function of affinity and antigen density, enabling nimotuzumab-CAR$^+$ T cells to maintain function to repeated challenge with elevated levels of EGFR, while cetuximab-CAR$^+$ T cells have reduced capacity to respond under conditions of serial stimulation.

Nimotuzumab- and cetuximab-CAR$^+$ T cells inhibit high-density EGFR$^+$ glioma growth *in vivo*

Because glioma cell lines express a median density of 240,000 molecules of EGFR/cell (22), U87^{med} (expressing approximately 340,000 molecules of EGFR/cell) modified to coexpress ffLuc-mKate were established as intracranial tumors in NSG mice to evaluate antitumor efficacy. Mice were stratified to receive no treatment, cetuximab-CAR$^+$ T cells, or nimotuzumab-CAR$^+$ T cells to evenly distribute relative tumor burden (Supplementary Fig. S5A). CAR$^+$ T cells were infused once a week for 3 weeks and relative tumor growth was monitored by BLI. CAR expression was similar cetuximab-CAR$^+$ T cells and nimotuzumab-CAR$^+$ T cells before infusion (Supplementary Fig. S5B). Cetuximab-CAR$^+$ T cells and nimotuzumab-CAR$^+$ T cells both significantly inhibited tumor growth (day 18; cetuximab-CAR, $P < 0.01$ and nimotuzumab-CAR, $P < 0.05$; Fig. 6A and B) and were not significantly different ($P > 0.05$). Mice receiving cetuximab-CAR$^+$ T cells exhibited toxicity manifested as rapid weight loss and lethargy, resulting in significant death of mice within 7 days of T-cell infusion. (6/14 mice, $P = 0.0006$; Fig. 6C). Overall, adoptive transfer of cetuximab-CAR$^+$ T cells did not statistically improve survival compared with untreated mice (untreated median survival = 88 days, cetuximab-CAR median survival = 105 days, $P = 0.19$; Fig. 6D). When only considering mice surviving 7 days after cetuximab-CAR$^+$ T-cell infusion, we noted improvement in survival of 75% of mice ($P = 0.0065$ relative to untreated mice). In contrast, nimotuzumab-CAR$^+$ T cells mediated effective tumor regression and extended survival in 4 of 7 of mice without apparent toxicity (untreated median survival = 88 days, nimotuzumab-CAR median survival = 158 days, $P = 0.0269$). Following 225 days, 2 of 7 mice in each treatment group were still living. These results demonstrate that cetuximab-CAR$^+$ T cells and nimotuzumab-CAR$^+$ T cells are both capable of controlling glioma with an high density of EGFR.

Nimotuzumab-CAR$^+$ T cells exhibit impaired targeting of low-density EGFR$^+$ cells *in vivo*

We next sought to determine whether CAR$^+$ T cells might exhibit a potential for undesired targeting of low EGFR density, by using parental U87 cells with low EGFR expression as a mimic for normal cells (Supplementary Fig. S5C). Treatment of mice with cetuximab-CAR$^+$ T cells resulted in significant reduction of U87 cells compared with untreated mice (day 25, $P < 0.01$; Fig. 7A and B), and significantly extended survival in 3 of 6 mice compared with mice receiving no treatment (untreated median survival = 38.5 days, cetuximab-CAR median survival = 53 days, $P = 0.015$; Fig. 7C). In contrast, administration of nimotuzumab-CAR$^+$ T cells did not significantly impact the growth of U87 compared with untreated mice (nimotuzumab-CAR, $P > 0.05$) and thus did not significantly improve survival (untreated median survival 38.5 days, nimotuzumab-CAR median survival 46 days, $P = 0.0969$). These data demonstrate that nimotuzumab-CAR$^+$ T cells, in contrast to cetuximab-CAR$^+$ T cells, do not mediate significant activity against parental U87 *in vivo*, which serve as a surrogate for normal tissue, demonstrating an effector profile consistent with reduced ability to target EGFR on normal cells.

Discussion

Aberrantly expressed antigens on tumors, such as EGFR on GBM, can be overexpressed relative to lower, basal levels on normal tissues. Taking advantage of this observation, we tuned CAR affinity to activate T cells based on the density of EGFR expression and demonstrated that a CAR with reduced affinity rendered T cells preferentially activated by high, but not low, density of EGFR. Our approach was based on the clinical toxicity exhibited by cetuximab and nimotuzumab, which recognize overlapping epitopes and exhibit different kinetics of binding to EGFR (13, 14). The lower affinity of nimotuzumab has been credited with absence of adverse events relative to cetuximab (15). Indeed, we revealed that a CAR species recognizing EGFR via the scFv derived from nimotuzumab exhibited a gradient of T-cell activation that directly correlated with density of expression of EGFR. In fact, as predicted by studies with nimotuzumab, nimotuzumab-CAR$^+$ T cells exhibited no apparent T-cell activation (absence of phosphorylation of MAPK molecules and cytokine production) in response to densities of EGFR found on normal tissues.

There are few studies addressing the role of scFv affinity in the therapeutic aptitude of CAR designs. Most recently, and in support of our findings, an EGFRvIII-specific CAR with reduced affinity has been reported with reduced binding to wild-type EGFR, and therefore reduced potential for normal tissue toxicity (28). A ROR1-specific CAR with increased affinity resulted in augmented T-cell function in response to TAA, which led to superior antitumor activity *in vivo* (29). Our study supports these findings in the situation of low antigen density on target cells, however, when antigen density is high on target cells, we found no benefit of increased scFv affinity. A series of CARs derived from a panel of HER2-specific mAbs with a range of K_d values demonstrated that the affinity of CAR above a minimum threshold required for activation did not improve T-cell response to targets with a range of HER2 densities (30).

While the affinity constant (K_d) is one measure used to describe the functional affinity of a CAR species, the relative contributions of on- and off-rates may account for disparate findings between these studies, as is likely the case with αβ TCR affinity in governing endogenous T-cell responses (31, 32). The reduced affinity constant of nimotuzumab is most impacted by a reduced on-rate of

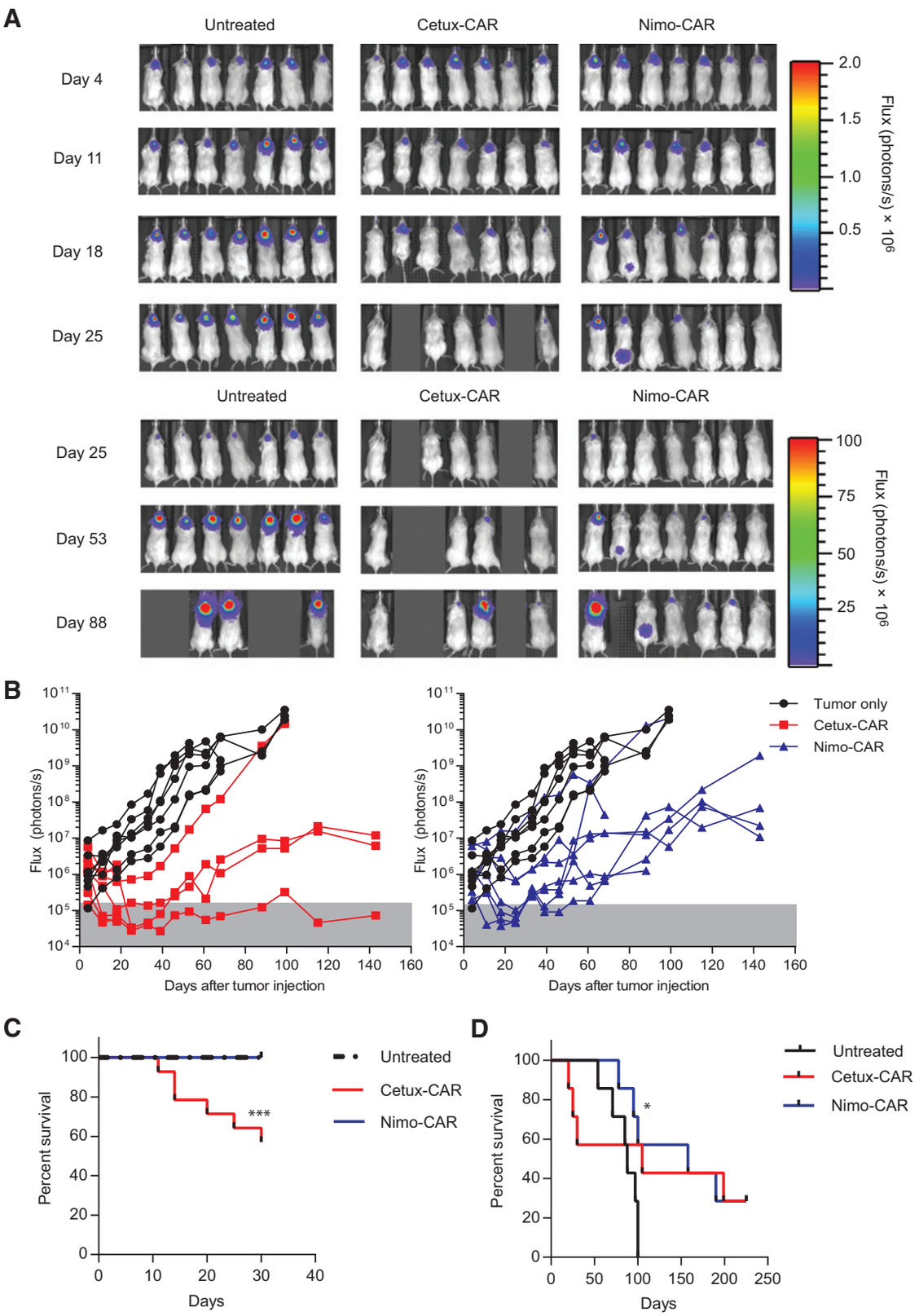

binding, requiring at least bivalent interaction to bind to target cells, which is more likely to occur in the presence of high antigen density. Thus, the capacity of the CAR to bind antigen at differing densities likely accounts for the superior ability of cetuximab-CAR compared with nimotuzumab-CAR to recognize low-density EGFR. Nimotuzumab and cetuximab bind highly overlapping epitopes, making it unlikely that magnitude of differences in CAR function are due solely to differences in epitope location; however, the contribution of this factor cannot be excluded.

Two parameters of TCR binding have been described that contribute to T-cell functional avidity: quality (binding affinity) and quantity (number of receptors engaged; refs. 12, 33). Increasing quantity of lower affinity TCRs can restore some T-cell functions, but not all, highlighting that some functions are dependent on quality versus quantity of activation signal. We observed a distinction between the quality and quantity of signaling mediated by cetuximab-CAR versus nimotuzumab-CAR. Nimotuzumab-CAR$^+$ T cells docking with glioma cells expressing high EGFR density demonstrated reduced phosphorylation of Erk1/2 and p38 compared with cetuximab-CAR$^+$ T cells, in spite of equivalent phosphorylation of Erk1/2 and p38 in response to CAR-L$^+$ EL4, yet maintained comparable functional responses. Because low-affinity TCRs can signal through transient, undetectable phosphorylation intermediates to culminate in functional T-cell response, it is possible a similar mechanism is responsible for this observation in nimotuzumab-CAR$^+$ T cells (23).

High-affinity TCRs and CARs can elicit impaired functional T-cell responses, due to prolonged interactions prohibiting serial triggering, which is necessary to generate a fully functional T-cell response (34–37). In CAR-modified T cells, however, the requirement for serial triggering has been overcome by expressing CAR at higher densities, reducing the need for serial triggering to activate T cells. Thus, any theoretical impairment of cetuximab-CAR function due to its high affinity may be masked by expression at high density on T cells. We observed that cetuximab-CAR was less capable of mounting a T-cell response upon re-exposure to EGFR, which was predicted by the downregulation of cetuximab-CAR after initial docking with EGFR. Similarly, cetuximab-CAR$^+$ T cells exhibited less proliferative capacity than nimotuzumab-CAR$^+$ T cells in response to high EGFR density. Signaling through engineered and endogenous TCRs of high affinity has been reported to cause functional anergy in T cells (38–40), so whether a reduced secondary response of cetuximab-CAR$^+$ T cells is due to loss of CAR and/or functional anergy remains to be elucidated.

Because cetuximab and nimotuzumab do not cross-react with murine EGFR, we measured deleterious binding of CAR$^+$ T cells to low density EGFR based upon implantation of parental U87 cells, which express low levels of EGFR and thus serve as a surrogate for normal human cells. We observed that adoptive transfer of cetuxiamb-CAR$^+$ T cells, but not nimotuzumab-CAR$^+$ T cells, could control growth of parental U87 cells. Therefore, T cells expressing a CAR with increased affinity for EGFR are likely to result in recognition of low levels of EGFR expression *in vitro* and *in vivo* leading to on-target, off-tissue toxicity. It is possible that nimotuzumab-CAR$^+$ T cells may result in outgrowth of low-density EGFR tumor escape variants, as described in studies with other CARs targeting GBM-associated antigens (41). Computational modeling based on extent and intensity of multiple antigens expressed on resected patient GBMs can inform design of a combination therapy utilizing CARs with multiple specificities to overcome this limitation.

Alternative approaches exist for reducing or avoiding the potential for CAR-mediated toxicity to TAA expressed on normal tissues. Expression of CAR from introduced mRNA species or activation of a suicide switch to result in death of infused T cells temporally limit CAR$^+$ T-cell presence to reduce toxicity, but both permanently negate CAR T-cell function and may undermine therapeutic efficacy (42–45). Limiting T-cell activation to CAR binding malignant cells can be achieved by coexpression of CARs with dissociated signaling domains targeting TAA only mutually expressed on malignant cells, such that binding of both CARs is needed to achieve a fully competent T-cell activation signal (46–48). However, requirement for expression of two antigens for efficient T-cell activation reduces the fraction of tumor capable of triggering CAR T cells, and a partial signal received from interaction of one CAR with TAA on normal tissue may be sufficient to mediate toxicity. Coexpression of a CAR activated in response to TAA and a CAR inhibitory in response to normal tissue antigen could minimize normal tissue toxicity (49); however, careful consideration of stoichiometric ratios of antigens on normal tissue is required. Our approach has merit in simplicity as only one TAA is targeted.

In conclusion, the weakness of the nimotuzumab-CAR affinity is its apparent strength. Our data support a new approach to designing genetically modified T cells to help them separate friend from foe by tuning scFv affinity to preferentially target the increased density of TAA. The relative inability of nimotuzumab-CAR$^+$ T cells to control U87 xenografts with low EGFR density *in vivo* combined with *in vitro* evidence that nimotuzumab-CAR$^+$ T cells are not activated in the presence of low-density EGFR suggest that nimotuzumab-CAR$^+$ T cells are favorably impaired in their ability to damage normal cells, especially relative to cetuximab-CAR$^+$ T cells. We cannot eliminate the possibility of nimotuzumab-CAR$^+$ T cells mediating some degree of on-target, off-tissue toxicity, therefore, initial clinical evaluation of nimotuzumab-CAR$^+$ T cells should be undertaken with suicide genes in patients with high-grade glioma via intracranial delivery of T cells as the central nervous system lacks notable EGFR expression (9), and may be extended to other cancers overexpressing EGFR, including bladder, cervical, esophageal, head and neck

Figure 6.
Nimotuzumab-CAR$^+$ (Nimo-CAR$^+$) and cetuximab-CAR$^+$ (Cetux-CAR$^+$) T cells inhibit high-density EGFR$^+$ glioma growth *in vivo*. A, serial BLI assessed relative size of tumor (introduced on day 0). B, relative tumor growth as assessed by serial BLI of tumor. Background luminescence (gray shading) was defined by BLI of mice with no tumors. Significant difference in BLI between mice with no treatment versus treatment ($n = 7$) with cetuximab-CAR$^+$ T cells ($n = 7$, $P < 0.01$) and no treatment ($n = 7$) versus treatment with nimotuzumab-CAR$^+$ T cells ($n = 7$, $P < 0.05$) at day 18, two-way ANOVA (Sidak post-test). C, survival of mice with U87^{med}-ffLuc-mKate intracranial xenografts from two independent experiments within 7 days of T-cell administration. Significant reduction in survival in cetuximab-CAR$^+$ T-cell–treated mice (8/14 surviving at day 26) relative to untreated mice (14/14 surviving at day 26) determined by the Mantel–Cox log-rank test, $P = 0.0006$. D, survival of mice with U87^{med}-ffLuc-mKate intracranial xenografts receiving no treatment, cetuximab-CAR$^+$ T cells, or nimotuzumab-CAR$^+$ T cells. Significant extension in survival in the nimotuzumab-CAR$^+$ T-cell treatment group determined by the Mantel–Cox log-rank test, $P = 0.027$.

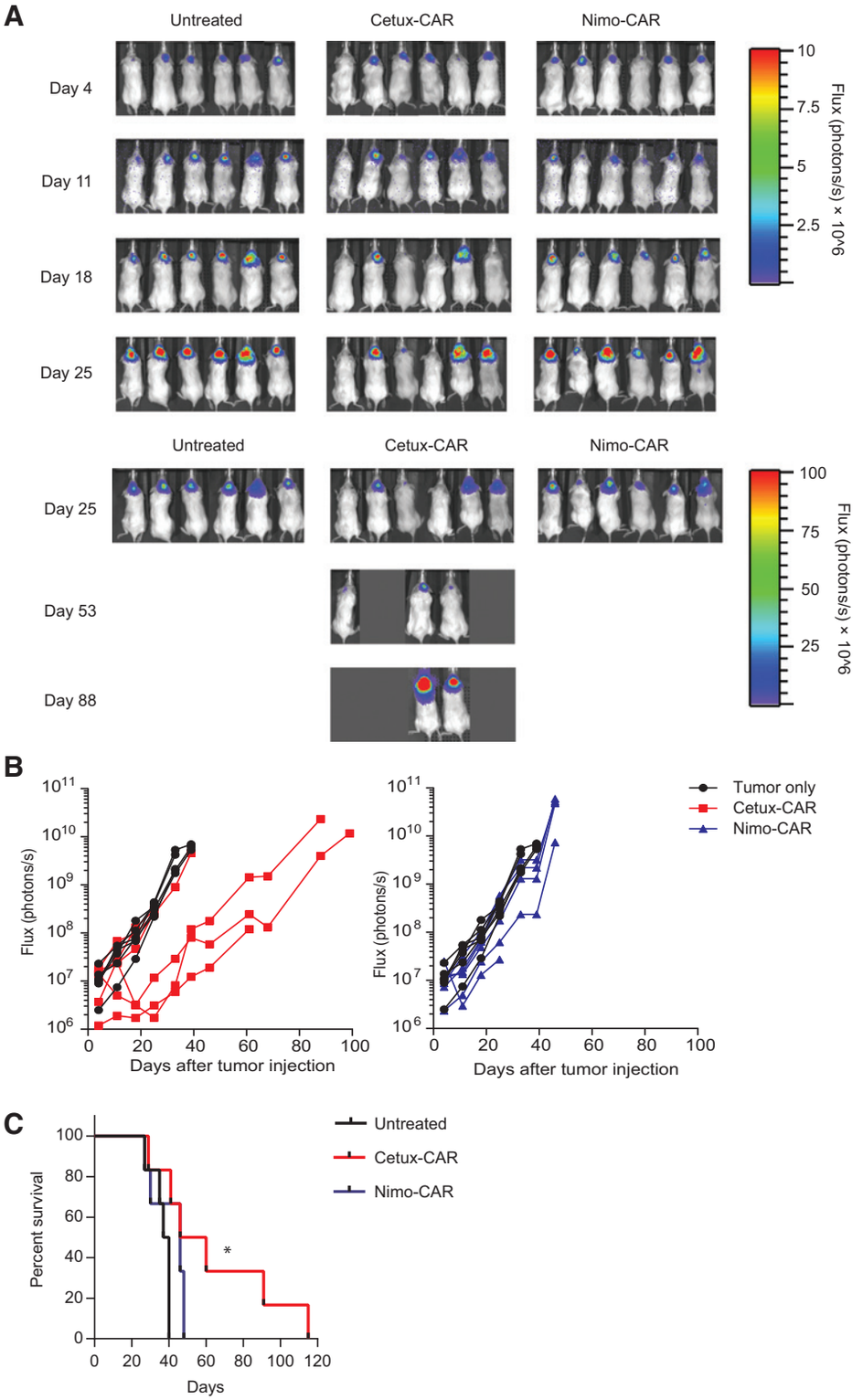

Figure 7.
Nimotuzumab-CAR$^+$ (Nimo-CAR$^+$) T cells exhibit impaired targeting of low-density EGFR cells *in vivo*. A, serial BLI assessed relative size of tumor. B, relative tumor growth as assessed by serial BLI of tumor. Significant difference in BLI between mice with no treatment ($n = 6$) versus treatment with cetuximab-CAR$^+$ (Cetux-CAR$^+$) T cells ($n = 6$, $P < 0.01$) reached at day 25, two-way ANOVA (Sidak post-test). C, survival of mice with U87-ffLuc-mKate intracranial xenografts receiving no treatment, cetuximab-CAR$^+$ T cells, or nimotuzumab-CAR$^+$ T cells. Significant extension in survival in the cetuximab-CAR$^+$ T-cell treatment group determined by Mantel–Cox log-rank test, $P = 0.0150$.

squamous cell, ovarian, breast, colorectal, gastric, endometrial, and non–small lung cell carcinomas (50).

Disclosure of Potential Conflicts of Interest

H.G. Caruso has ownership interest (including patents) in Intrexon and Ziopharm Oncology. L.V. Hurton has ownership interest (including patents) in Intrexon Corporation and Ziopharm Oncology. A. Najjar has ownership interest in Intrexon and Ziopharm. D. Rushworth has ownership interest in Ziopharm and Intrexon. S. Olivares has ownership interest in Intrexon and Ziopharm. S. Ang has ownership interest in Intrexon and Ziopharm. K. Switzer has ownership interest (including patents) in Intrexon and Ziopharm. T. Mi has ownership interest in Ziopharm and Intrexon. H. Singh has ownership interest (including patents) in Intrexon and Ziopharm. D.A. Lee has ownership interest (including patents) in Intrexon, Ziopharm, and Cyto-Sen. R. Champlin has ownership interest in Intrexon and Ziopharm. L.J.N Cooper reports receiving commercial research support from Immatics US, has speakers' bureau honoraria from Miltenyi Biotec, and has ownership interest (including patents) in Intrexon, Ziopharm Oncology, and is a consultant/advisory board member for Targazyme, Inc. No potential conflicts of interests were disclosed by the other authors.

Disclaimer

The content is solely the responsibility of the authors and does not necessarily represent the official views of the NIH.

Authors' Contributions

Conception and design: H.G. Caruso, S. Ang, R.E. Champlin, L.J.N Cooper
Development of methodology: H.G. Caruso, D. Rushworth, S. Ang, H. Huls, D.A. Lee, L.J.N Cooper
Acquisition of data (provided animals, acquired and managed patients, provided facilities, etc.): H.G. Caruso, A. Najjar, T. Mi, K. Switzer, H. Singh, A.B. Heimberger, L.J.N Cooper
Analysis and interpretation of data (e.g., statistical analysis, biostatistics, computational analysis): H.G. Caruso, H. Singh, A.B. Heimberger, L.J.N Cooper
Writing, review, and/or revision of the manuscript: H.G. Caruso, D.A. Lee, A.B. Heimberger, R.E. Champlin, L.J.N Cooper
Administrative, technical, or material support (i.e., reporting or organizing data, constructing databases): L.V. Hurton, D. Rushworth, L.J.N Cooper
Study supervision: D.A. Lee, A.B. Heimberger, R.E. Champlin, L.J.N Cooper
Other (designed Cetux-CAR and Nimo-CAR structures in Sleeping Beauty vectors): S. Olivares

Acknowledgments

The authors thank flow cytometry and cellular imaging core facilities at MDACC (supported by CA016672). The authors also thank P. Hackett (University of Minnesota) for his assistance with SB system, O. Bogler (MDACC) for his gift of U87 cell line overexpressing EGFR ($U87^{high}$), F. Lang, V. Henry, and L. Holmes for training and implementation of guide screw glioma xenograft model, and J. Moyes and G. McNamara for editing. In memory of Patricia Ann Cooper.

Grant Support

This work was supported by a Cancer Center Core Grant (CA16672); RO1 (CA124782, CA120956, CA141303); P01 (CA148600); Center for Clinical and Translational Sciences, which is funded by National Center for Advancing Translational Sciences of the NIH under Award Number TL1TR000369; SPORE (P50 CA136411); Albert J Ward Foundation; Alex Lemonade Stand Foundation; American Legion Auxiliary, Burroughs Wellcome Fund; Cancer Answers; Cancer Prevention and Research Institute of Texas; Charles B. Goddard Foundation of Texas; CLL Global Research Foundation; DARPA (Defense Sciences Office); Department of Defense; Estate of Noelan L. Bibler; Gillson Longenbaugh Foundation; Harry T. Mangurian, Jr, Fund for Leukemia Immunotherapy; Khalifa Bin Zayed Al Nahyan Foundation; Leukemia and Lymphoma Society; Lymphoma Research Foundation; Miller Foundation; Moon Shot program at MDACC, Mr. Herb Simons; Mr. and Mrs. Joe H. Scales; Mr. Thomas Scott; National Foundation for Cancer Research; Pediatric Cancer Research Foundation; Sheikh Khalifa Bin Zayed Al Nahyan Institute for Personalized Cancer Therapy; R.W. Butcher Foundation, MDACC Sister Institution Network Fund and Moon Shot Fund; William Lawrence and Blanche Hughes Children's Foundation.

The costs of publication of this article were defrayed in part by the payment of page charges. This article must therefore be hereby marked *advertisement* in accordance with 18 U.S.C. Section 1734 solely to indicate this fact.

Received January 14, 2015; revised April 21, 2015; accepted June 13, 2015; published online September 1, 2015.

References

1. Porter DL, Levine BL, Kalos M, Bagg A, June CH. Chimeric antigen receptor-modified T cells in chronic lymphoid leukemia. N Engl J Med 2011;365:725–33.
2. Grupp SA, Kalos M, Barrett D, Aplenc R, Porter DL, Rheingold SR, et al. Chimeric antigen receptor-modified T cells for acute lymphoid leukemia. N Engl J Med 2013;368:1509–18.
3. Maude SL, Frey N, Shaw PA, Aplenc R, Barrett DM, Bunin NJ, et al. Chimeric antigen receptor T cells for sustained remissions in leukemia. N Engl J Med 2014;371:1507–17.
4. Ostrom QT, Gittleman H, Liao P, Rouse C, Chen Y, Dowling J, et al. CBTRUS statistical report: primary brain and central nervous system tumors diagnosed in the United States in 2007–2011. Neuro Oncol 2014;16 Suppl 4:iv1–63.
5. Johnson DR, O'Neill BP. Glioblastoma survival in the United States before and during the temozolomide era. J Neurooncol 2012;107:359–64.
6. Nicholas MK, Lukas RV, Jafri NF, Faoro L, Salgia R. Epidermal growth factor receptor - mediated signal transduction in the development and therapy of gliomas. Clin Cancer Res 2006;12:7261–70.
7. Stommel JM, Kimmelman AC, Ying H, Nabioullin R, Ponugoti AH, Wiedemeyer R, et al. Coactivation of receptor tyrosine kinases affects the response of tumor cells to targeted therapies. Science 2007;318:287–90.
8. Lo HW. EGFR-targeted therapy in malignant glioma: novel aspects and mechanisms of drug resistance. Curr Mol Pharmacol 2010;3:37–52.
9. Yano S, Kondo K, Yamaguchi M, Richmond G, Hutchison M, Wakeling A, et al. Distribution and function of EGFR in human tissue and the effect of EGFR tyrosine kinase inhibition. Anticancer Res 2003;23:3639–50.
10. Lenz HJ. Anti-EGFR mechanism of action: antitumor effect and underlying cause of adverse events. Oncology 2006;20(5 Suppl 2):5–13.
11. Corse E, Gottschalk RA, Allison JP. Strength of TCR-peptide/MHC interactions and in vivo T cell responses. J Immunol 2011;186:5039–45.
12. Tan MP, Gerry AB, Brewer JE, Melchiori L, Bridgeman JS, Bennett AD, et al. TCR binding affinity governs the functional profile of cancer-specific CD8 T cells. Clin Exp Immunol 2015;180:255–70.
13. Talavera A, Friemann R, Gomez-Puerta S, Martinez-Fleites C, Garrido G, Rabasa A, et al. Nimotuzumab, an antitumor antibody that targets the epidermal growth factor receptor, blocks ligand binding while permitting the active receptor conformation. Cancer Res 2009;69:5851–9.
14. Garrido G, Tikhomirov IA, Rabasa A, Yang E, Gracia E, Iznaga N, et al. Bivalent binding by intermediate affinity of nimotuzumab: a contribution to explain antibody clinical profile. Cancer Biol Ther 2011;11:373–82.
15. Perez R, Moreno E, Garrido G, Crombet T. EGFR-targeting as a biological therapy: understanding Nimotuzumab's clinical effects. Cancers 2011;3:2014–31.
16. Singh H, Manuri PR, Olivares S, Dara N, Dawson MJ, Huls H, et al. Redirecting specificity of T-cell populations for CD19 using the Sleeping Beauty system. Cancer Res 2008;68:2961–71.
17. Rushworth D, Jena B, Olivares S, Maiti S, Briggs N, Somanchi S, et al. Universal artificial antigen presenting cells to selectively propagate T cells expressing chimeric antigen receptor independent of specificity. J Immunother 2014;37:204–13.

18. Suhoski MM, Golovina TN, Aqui NA, Tai VC, Varela-Rohena A, Milone MC, et al. Engineering artificial antigen-presenting cells to express a diverse array of co-stimulatory molecules. Mol Ther 2007;15:981–8.
19. Romano P, Manniello A, Aresu O, Armento M, Cesaro M, Parodi B. Cell Line Data Base: structure and recent improvements towards molecular authentication of human cell lines. Nucleic Acids Res 2009;37: D925–32.
20. Diaz Miqueli A, Blanco R, Garcia B, Badia T, Batista AE, Alonso R, et al. Biological activity in vitro of anti-epidermal growth factor receptor monoclonal antibodies with different affinities. Hybridoma 2007;26:423–31.
21. Hollenberg MD, Cuatrecasas P. Insulin and epidermal growth factor. Human fibroblast receptors related to deoxyribonucleic acid synthesis and amino acid uptake. J Biol Chem 1975;250:3845–53.
22. Bigner SH, Humphrey PA, Wong AJ, Vogelstein B, Mark J, Friedman HS, et al. Characterization of the epidermal growth factor receptor in human glioma cell lines and xenografts. Cancer Res 1990;50:8017–22.
23. Rosette C, Werlen G, Daniels MA, Holman PO, Alam SM, Travers PJ, et al. The impact of duration versus extent of TCR occupancy on T cell activation: a revision of the kinetic proofreading model. Immunity 2001;15:59–70.
24. Yachi PP, Ampudia J, Zal T, Gascoigne NR. Altered peptide ligands induce delayed CD8-T cell receptor interaction–a role for CD8 in distinguishing antigen quality. Immunity 2006;25:203–11.
25. Karawajew L, Jung G, Wolf H, Micheel B, Ganzel K. A flow cytometric long-term cytotoxicity assay. J Immunol Methods 1994;177:119–30.
26. Stanke J, Hoffmann C, Erben U, von Keyserling H, Stevanovic S, Cichon G, et al. A flow cytometry-based assay to assess minute frequencies of CD8+ T cells by their cytolytic function. J Immunol Methods 2010;360: 56–65.
27. Cai Z, Kishimoto H, Brunmark A, Jackson MR, Peterson PA, Sprent J. Requirements for peptide-induced T cell receptor downregulation on naive CD8+ T cells. J Exp Med 1997;185:641–51.
28. Johnson LA, Scholler J, Ohkuri T, Kosaka A, Patel PR, McGettigan SE, et al. Rational development and characterization of humanized anti-EGFR variant III chimeric antigen receptor T cells for glioblastoma. Sci Transl Med 2015;7:275ra22.
29. Hudecek M, Lupo-Stanghellini MT, Kosasih PL, Sommermeyer D, Jensen MC, Rader C, et al. Receptor affinity and extracellular domain modifications affect tumor recognition by ROR1-specific chimeric antigen receptor T cells. Clin Cancer Res 2013;19:3153–64.
30. Chmielewski M, Hombach A, Heuser C, Adams GP, Abken H. T cell activation by antibody-like immunoreceptors: increase in affinity of the single-chain fragment domain above threshold does not increase T cell activation against antigen-positive target cells but decreases selectivity. J Immunol 2004;173:7647–53.
31. Stone JD, Chervin AS, Kranz DM. T-cell receptor binding affinities and kinetics: impact on T-cell activity and specificity. Immunology 2009;126: 165–76.
32. Govern CC, Paczosa MK, Chakraborty AK, Huseby ES. Fast on-rates allow short dwell time ligands to activate T cells. Proc Natl Acad Sci U S A 2010;107:8724–9.
33. Gottschalk RA, Hathorn MM, Beuneu H, Corse E, Dustin ML, Altan-Bonnet G, et al. Distinct influences of peptide-MHC quality and quantity on in vivo T-cell responses. Proc Natl Acad Sci U S A 2012;109:881–6.
34. Thomas S, Xue SA, Bangham CR, Jakobsen BK, Morris EC, Stauss HJ. Human T cells expressing affinity-matured TCR display accelerated responses but fail to recognize low density of MHC-peptide antigen. Blood 2011;118:319–29.
35. Chervin AS, Stone JD, Soto CM, Engels B, Schreiber H, Roy EJ, et al. Design of T-cell receptor libraries with diverse binding properties to examine adoptive T-cell responses. Gene Ther 2013;20:634–44.
36. Weijtens ME, Hart EH, Bolhuis RL. Functional balance between T cell chimeric receptor density and tumor associated antigen density: CTL mediated cytolysis and lymphokine production. Gene Ther 2000;7: 35–42.
37. Turatti F, Figini M, Balladore E, Alberti P, Casalini P, Marks JD, et al. Redirected activity of human antitumor chimeric immune receptors is governed by antigen and receptor expression levels and affinity of interaction. J Immunother 2007;30:684–93.
38. Corse E, Gottschalk RA, Krogsgaard M, Allison JP. Attenuated T cell responses to a high-potency ligand *in vivo*. PLoS Biol 2010;8:e100481.
39. Janicki CN, Jenkinson SR, Williams NA, Morgan DJ. Loss of CTL function among high-avidity tumor-specific CD8+ T cells following tumor infiltration. Cancer Res 2008;68:2993–3000.
40. Lim DG, Hollsberg P, Hafler DA. Strength of prior stimuli determines the magnitude of secondary responsiveness in CD8+ T cells. Cell Immunol 2002;217:36–46.
41. Hegde M, Corder A, Chow KK, Mukherjee M, Ashoori A, Kew Y, et al. Combinational targeting offsets antigen escape and enhances effector functions of adoptively transferred T cells in glioblastoma. Mol Ther 2013;21:2087–101.
42. Barrett DM, Liu X, Jiang S, June CH, Grupp SA, Zhao Y. Regimen-specific effects of RNA-modified chimeric antigen receptor T cells in mice with advanced leukemia. Hum Gene Ther 2013;24:717–27.
43. Singh N, Liu X, Hulitt J, Jiang S, June CH, Grupp SA, et al. Nature of tumor control by permanently and transiently modified GD2 chimeric antigen receptor T cells in xenograft models of neuroblastoma. Cancer Immunol Res 2014;2:1059–70.
44. Beatty GL, Haas AR, Maus MV, Torigian DA, Soulen MC, Plesa G, et al. Mesothelin-specific chimeric antigen receptor mRNA-engineered T cells induce anti-tumor activity in solid malignancies. Cancer Immunol Res 2014;2:112–20.
45. Di Stasi A, Tey SK, Dotti G, Fujita Y, Kennedy-Nasser A, Martinez C, et al. Inducible apoptosis as a safety switch for adoptive cell therapy. N Engl J Med 2011;365:1673–83.
46. Wilkie S, van Schalkwyk MC, Hobbs S, Davies DM, van der Stegen SJ, Pereira AC, et al. Dual targeting of ErbB2 and MUC1 in breast cancer using chimeric antigen receptors engineered to provide complementary signaling. J Clin Immunol 2012;32:1059–70.
47. Lanitis E, Poussin M, Klattenhoff AW, Song D, Sandaltzopoulos R, June CH, et al. Chimeric antigen receptor T cells with dissociated signaling domains exhibit focused anti-tumor activity with reduced potential for toxicity. Cancer Immunol Res 2013;1:43–53.
48. Kloss CC, Condomines M, Cartellieri M, Bachmann M, Sadelain M. Combinatorial antigen recognition with balanced signaling promotes selective tumor eradication by engineered T cells. Nat Biotechnol 2013;31:71–5.
49. Fedorov VD, Themeli M, Sadelain M. PD-1- and CTLA-4-based inhibitory chimeric antigen receptors (iCARs) divert off-target immunotherapy responses. Sci Transl Med 2013;5:215ra172.
50. Nicholson RI, Gee JM, Harper ME. EGFR and cancer prognosis. Eur J Cancer 2001;37 Suppl 4:S9–15.

Tuning Sensitivity of CAR to EGFR Density Limits Recognition of Normal Tissue While Maintaining Potent Antitumor Activity

Hillary G. Caruso, Lenka V. Hurton, Amer Najjar, et al.

Cancer Res 2015;75:3505-3518.